Journal of Engineering for Gas Turbines and Power. Received June 18, 2016;
Accepted manuscript posted November 22, 2016. DOI:10.1115/1.4035283

Journal of Engineering for Gas Turbines and Power,
Volume 139, Issue 6, 062601-1-9
DOI: 10.1115/1.4035283

An automated approach to nacelle parameterization using intuitive class shape transformation curves

Robert Christie*
Propulsion Engineering Centre
School of Aerospace,
Transport, and Manufacturing,
Cranfield University
Bedfordshire, MK43 0AL, UK
Email: r.christie@cranfield.ac.uk

Alexander Heidebrecht

Propulsion Engineering Centre
School of Aerospace,
Transport, and Manufacturing,
Cranfield University
Bedfordshire, MK43 0AL, UK

David MacManus

Propulsion Engineering Centre
School of Aerospace, Transport, and Manufacturing
Cranfield University
Bedfordshire, MK43 0AL, UK

ABSTRACT

A tool to create parametric aerodynamic shapes using intuitive design variables based on class shape transformation curves is presented. To enable this, a system has been developed which accepts arbitrary constraints and automatically derives the analytical expressions which describe the corresponding class shape transformation curves. Parametric geometry definitions for fan cowl and intake aero-lines were developed using the generalized method. CFD analysis of the fan cowl shows that despite the simple geometry definition its performance characteristics are close to what would be expected of a finished design. The intake geometry was generated in a similar way and met the typical performance metrics for conventional intakes. This demonstrates the usefulness of the tool to quickly and robustly produce parametric aero-lines with good aerodynamic properties, using relatively simple intuitive design variables.

Nomenclature

Roman Symbols

a	An element in the matrix of coefficients
A	Matrix of coefficients
b	An element in the matrix of constant terms
B	Matrix of constant terms
C	Class function
c	Chord length
c_D	drag coefficient
$c_{D,hi}$	nacelle drag coefficient related to highlight area
C_{Lmax}	Maximum lift configuration
D_{fan}	Fan Diameter

*Address all correspondence to this author.

DC_{60}	Total Pressure Distortion Parameter
f_{max}	Non-dimensional position of maximum nacelle radius
i	Index of summation
K	Binomial coefficient
k	Order of derivative
$L^2 - norm$	The Euclidean norm
L_{intake}	Intake length
M	Mach number
M_{ISEN}	Isentropic Mach number
N	Upper bound on summation
n	Bernstein polynomial order
N_1	First exponent in the class function
N_2	Second exponent in the class function
N_{con}	Number of constraints
$P_{0,fan\,face}$	Fan face mean total pressure
P_0	Total pressure
P_{60}	Mean total pressure in the 60^o sector with the lowest mean total pressure
q	Dynamic pressure
Q_{fan}	Quasi-non-dimensional flow parameter at the nominal fan face
R	Radius of curvature
r	radial coordinate
r_{hi}	highlight radius
r_{if}	initial forebody radius: radius of curvature at nacelle highlight
r_{max}	maximum nacelle radius
r_{te}	nacelle trailing edge radius
S	Shape function
x	Abscissa
X	Matrix of solutions
x	axial coordinate
y	Ordinate

Abbreviations

AIP	Aerodynamic interface plane
AR	Lip aspect ratio
BP	Bernstein Polynomial
bp	Bernstein polynomial weighting coefficient
CFD	Computational Fluid Dynamics
CR	Intake contraction ratio
CRM	Common Research Model
CST	Class-Shape Transformation
FPR	Fan Pressure Ratio
iCST	Intuitive Class Shape Transformation
IPR	Intake Pressure Recovery
le	Leading edge
LMFIT	Non-Linear Least-Square Minimization and Curve-Fitting for Python
MFCR	Mass-flow capture ratio
PARSEC	Parameterization method for airfoil sections
TDC	Top Dead Centre
te	Trailing edge
TFN	Through-flow nacelle

Greek Symbols

α	Angle of attack
β	Boattail angle
δ_{Zte}	Radial offset between highlight and trailing edge
κ	Curvature
ψ	Non-dimensional abscissa
ξ	Non-dimensional ordinate

INTRODUCTION

External aerodynamic shapes can be represented in a number of ways. The most basic approach is to construct the shape from a point cloud. This method however requires a large number of design variables to guarantee a smooth and accurate shape [1]. To limit the amount of design parameters, the aerodynamic shape can be defined by a parametric curve. The choice of parameterization method has a profound effect on the design space and is a key decision in the design process [2]. Class shape transformation (CST) curves are known from wing profile design to create aerodynamically useful shapes. [3,4]. This method is capable of producing a wide range of aerodynamic shapes including intake and fan cowl aero-lines [3] in a universal way with a small number of design variables. The CST approach however lacks intuitiveness of the design parameters for geometrical and physical understanding of the constraints. This is required by a user in exploring the design space and in the application of optimization constraints. This drawback has been addressed for a specific set of constraints [5]. The intuitiveness of the parameterization method for airfoil sections (PARSEC) [6] was combined with the highly flexible CST parameterization method. This intuitive CST (iCST) approach is a transformation of the CST parameterization method to a full set of intuitive parameters by a transformation matrix [5]. The current work provides a generalization on this iCST approach. A system has been developed which analytically calculates the transformation matrix for a set of arbitrary constraints. This generalization of the iCST method has then been implemented in a Python based geometry tool. The usefulness of the generalized method for fan cowl and intake aero-lines is then investigated. Representative fan cowl and intake aero-lines are constructed based on the NASA common research model (CRM) [7]. Nacelle drag characteristics are investigated through 2D axisymmetric Computational Fluid Dynamics (CFD), while the intake performance is assessed at high incidence with 3D CFD.

METHODOLOGY

Firstly the analytical approach to the creation of a transformation matrix for intuitive class shape transformation parameterization will be discussed. The approach is illustrated with an example fan cowl parameterization. Details of the CFD methods and aerodynamic performance metrics used to assess fan cowl and intake parametric geometries are then presented.

CST methodology

Class-Shape Transformation (CST) parameterization [3] represents a geometry by the product of a class function, $C(\psi)$, and a shape function, $S(\psi)$. The start and end points of all curves constructed with a class and shape function have equal ordinates. An additional term, $(\psi\Delta\xi_{te})$, is included to modify the end-point's ordinate [3]:

$$\xi(\psi) = S(\psi)C(\psi) + \psi\Delta\xi_{te} \;;\; \xi = \frac{y}{c} \;,\; \psi = \frac{x}{c} \tag{1}$$

The basic profile is defined by the class function. One set of class functions which describes basic external aerodynamic shapes through different exponent combinations takes the form [3]:

$$C_{N_2}^{N_1}(\psi) = \psi^{N_1}[1-\psi]^{N_2} \;\; for \; 0 \leq \psi \leq 1 \tag{2}$$

Equation 2 can be used to describe bi-convex ($C_{1.0}^{1.0}$), elliptic ($C_{0.5}^{0.5}$) and round-nosed ($C_{0.5}^{1.0}$) airfoil shapes as well as other common external aerodynamic shapes such as a Sears-Haack body ($C_{0.75}^{0.75}$) or a cone ($C_{0.+}^{1.0}$). The class function is modified by the shape function. Bernstein polynomials (Eq. 3) are commonly employed as the shape function [3–5].

$$BP(\psi) = \sum_{i=0}^{N} \left[K_{i,n} \cdot \left(\psi^i \cdot (1-\psi)^{n-1} \right) \right] \;;\; K_{i,n} = \frac{n!}{i!(n-1)!} \tag{3}$$

They are stable, robust and importantly form a partition of unity, i.e., the $n+1$ Bernstein polynomials of order n sum to one. The shape function can then be manipulated by the variation of Bernstein polynomial coefficients (Eq. 4) which in turn modifies the final profile (Figures 1 and 2).

$$S(\psi) = \sum_{i=0}^{N} \left[bp_i \cdot K_{i,n} \cdot \left(\psi^i \cdot (1-\psi)^{n-1} \right) \right] \tag{4}$$

The mathematically smooth behavior of Bernstein polynomial shape functions and their inherent curvature continuity make

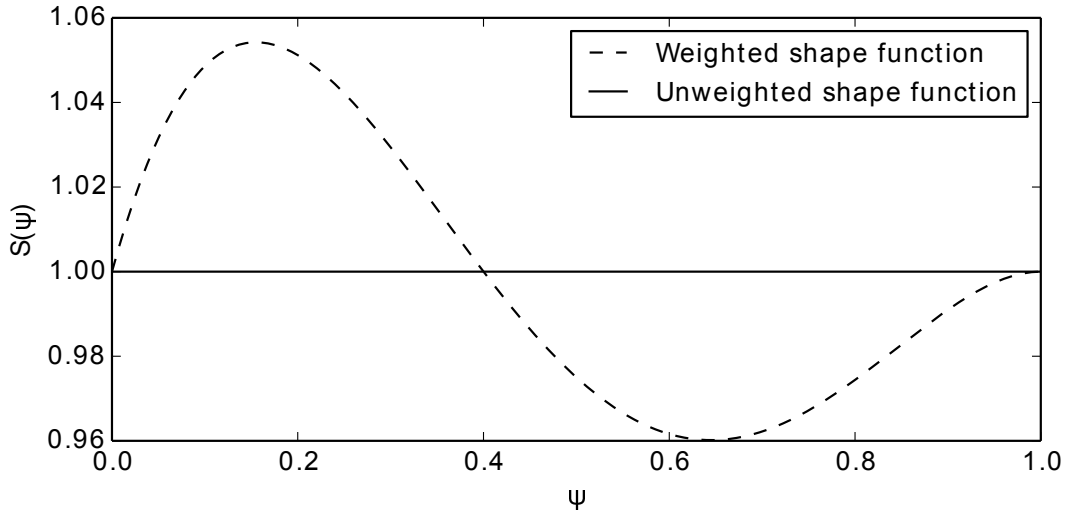

Fig. 1: Perturbation of the shape function by variation of the Bernstein polynomial weighting coefficients

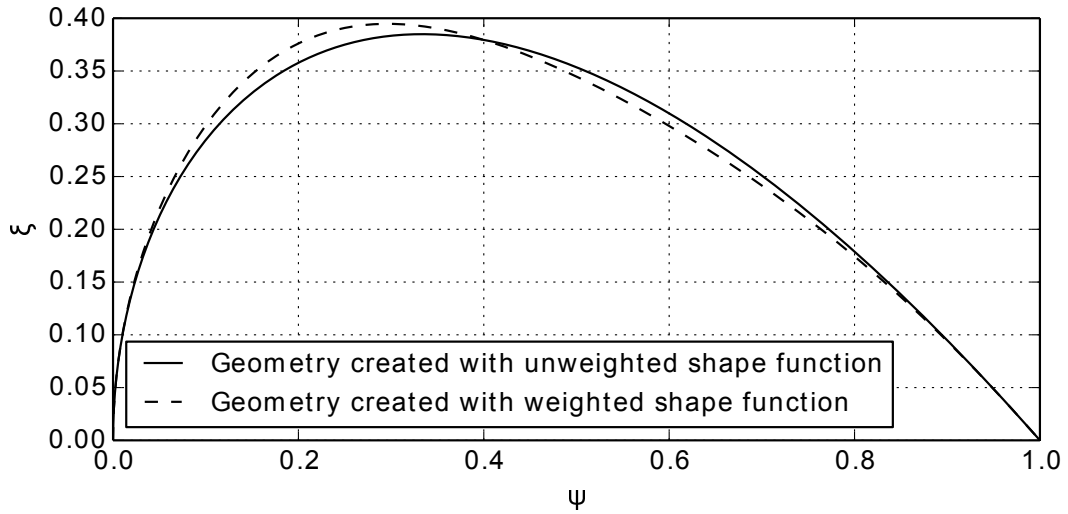

Fig. 2: Geometry formed using a unit shape function and a shape function perturbed by Bernstein polynomial weighting coefficients (Figure 1)

this system ideal for aerodynamic optimization work. However the design relies on the manipulation of the Bernstein polynomial weighting coefficients which are not aerodynamically intuitive. To allow a design engineer to explore the design space and set up constraints for optimization process the design parameters need to be physically intuitive. The Bernstein polynomial coefficients can be analytically calculated from intuitive variables through the construction of a transformation matrix. This has been carried out for a specific set of constraints [5]. However for each set of constraints a new transformation is required. Done manually this is a time consuming process. To rectify this a general method has been formulated which works with arbitrary constraints. This general method has then been implement in a Python based geometry generation tool. An automatic system to generate and solve these linear sets of equations has been developed. An arbitrary number of constraints (N_{con}) can be specified. The order of the resultant CST curve is then $N_{con} - 1$. Position, gradient and derivatives up to the nth degree can be set. Compound constraints such as curvature, radius of curvature and their derivatives can also be imposed (Appendix A). For each constraint the only required inputs are its magnitude, $\zeta^{(k)}$, and abscissa, ψ. Then Eq. 5 is rearranged to isolate the Bernstein polynomial weighting coefficients. The function's coefficients and constant terms can then be analytically extracted. A Python symbolic math module [8] can then be employed to solve the class function and its derivatives. The shape function and its derivatives can be solved by using the fact that derivatives of the kth degree Bernstein

polynomials are polynomials of degree $k-1$ and can be written as a linear combination of Bernstein polynomials (Eq. 6).

$$\xi^{(k)}(\psi) = \left[\sum_{i=0}^{N}\left[bp_i K_{i,n}\left(\psi^i(1-\psi)^{n-1}\right)\right]C(\psi) + \psi\Delta\xi_{te}\right]^{(k)} \tag{5}$$

$$\frac{d}{d\psi}BP_{i,n}(\psi) = n[BP_{k-1,n-1}(\psi) - BP_{k,n-1}(\psi)] \tag{6}$$

A linear set of equations is then constructed with the extracted coefficients and constant terms (Eq. 7).

$$\mathbf{A}\cdot\mathbf{X} = \mathbf{B} \tag{7}$$

This analytical creation of the transformation matrix for an arbitrary set of constraints allows curve parameterizations to be quickly and easily tested. As the analytical expressions for the produced profiles are available, detailed analytical curvature analysis can be performed. These methods have been implemented in a Python based geometry generation tool. A well-constructed parameterization method should be able to represent a large design space including existing geometries. To allow the representation of existing geometries an inverse fitting approach has been implemented which utilizes the LMFIT optimizer [9] in Python to minimize the $L^2 - norm$. The fitting of curves to existing shapes can be used to assess the order of CST curve required to capture a meaningful amount of the design space. To enable the comparison of CST curves at the same order a method to raise the order of a Bernstein polynomial has been implemented in Python. This method utilizes the fact that any Bernstein polynomial of degree less than n can be written as a linear combination of Bernstein polynomials of degree n. This allows the refinement of an existing CST parameterisation. The parametric definition of the produced profiles can easily be exported to CAD packages for accurate 3D modeling has also been implemented in the Python based tool. Compatibility with NX Unigraphics has been established with the ability to export an NX expressions file which describes the geometry.

Example test case

To illustrate how the transformation matrix between the Bernstein polynomial weighting coefficients and the intuitive design parameters is established, an example fan cowl construction is considered. The aim of this parametric geometry is to represent fan cowl shapes in a preliminary design context, which means it needs to function on the basis of very few input parameters, and it should be close in performance to a finished design.

For this, the open-source through-flow-nacelle (TFN) of the Common Research Model (CRM) [7] was used. The fan cowl sideline were extracted and used as a baseline for a comparison between an existing design and a reconstruction which employs an intuitive parameterisation and the main dimensions of the original geometry. While it cannot be expected that the parametric geometry is an improvement over the original, a good low-order geometry should result in a shape which has a consistent offset compared to a finished design. For fan cowl shapes, this holds for aerodynamic performance as well as for the internal volume it affords the designer to accommodate auxiliary units or a thrust reverser. The geometry fitting and comparison is shown in this section while the aerodynamic properties are discussed in the Results section of this paper.

The main geometric parameters from the original geometry were extracted, and are shown in Table 1. The parameters in Table 1 were non-dimensionalised (Eq. 1) and translated into the numerical constraints shown in Table 2, in the following fashion: The first three parameters define the positions of the fan cowl curve endpoints, (Constraints C.1 and C.2). These constraints do not influence the Bernstein polynomial weighting coefficients and do not count towards the order of the resultant Bernstein polynomials. r_{if} is taken directly as the radius of curvature at the leading edge and β as the boattail angle for Eq. 8 (Constraints C.3 and C.7). The location of maximum radius and r_{max} itself are translated into one constraint on the value of the curve (Constraint C.4) and another on the tangent (Constraint C.5) which is horizontal at the point of maximum radius. In addition to these, another constraint was added, which set curvature at the trailing edge to be zero. This is equivalent to setting the second derivative of the curve to zero (Constraint C.6). Constraints C.3 to C.7 then describe a fourth order Bernstein polynomial curve with five Bernstein polynomial weighting coefficients. This fan cowl parameterisation [10] uses a round nose airfoil as a class function ($C_{0.5}^{1.0}$). For this class function the first and last Bernstein polynomial weighting coefficients are a function of the leading edge radius of curvature and the trailing edge angle and offset (Eq. 8) and can be solved directly. Equation 5 can be used to set up the matrix of coefficients (Eq. 9) and the matrix of constant terms (Eq 10) to solve for the remaining three Bernstein polynomial weighting coefficients; bp_1, bp_2 and bp_3 (Eq. 11).

$$bp_0 = \sqrt{\frac{2R_{le}}{c}}\ ;\ bp_n = \tan(\beta) + \frac{\delta z_{te}}{c} \tag{8}$$

#	Name	Value	Description
P.1	r_{hi}	$1.658m$	highlight radius
P.2	r_{te}	$1.469m$	trailing edge radius
P.3	l_{nac}	$5.966m$	nacelle length
P.4	r_{if}	$0.053m$	initial forebody radius
P.5	r_{max}	$2.000m$	maximum radius
P.6	f_{max}	0.379	location of max. radius (fraction of l_{nac})
P.7	β	13.27°	boattail angle

Table 1: Main parameters of the CRM TFN sideline geometry

#	Type	ψ	$\xi^{(k)}(\psi)$	Influences
C.1	Position	0.000	0.278	–
C.2	Position	1.000	0.246	–
C.3	Radius of curvature	0.000	8.9×10^{-3}	bp_0
C.4	Position	0.379	0.335	bp_1, bp_2, bp_3
C.5	Gradient	0.379	0.000	bp_1, bp_2, bp_3
C.6	2nd Derivative	1.000	0.000	bp_1, bp_2, bp_3
C.7	Gradient	1.000	0.236	bp_n

Table 2: Fan cowl CST example

$$\mathbf{A} = \begin{bmatrix} a_{1,1} & a_{1,2} & a_{1,3} \\ a_{2,1} & a_{2,2} & a_{2,3} \\ a_{3,1} & a_{3,2} & a_{3,3} \end{bmatrix} \tag{9}$$

$$\mathbf{B} = \begin{bmatrix} b_{1,0} & b_{2,0} & b_{3,0} \end{bmatrix}^T \tag{10}$$

$$\mathbf{X} = \begin{bmatrix} bp_1 & bp_2 & bp_3 \end{bmatrix}^T \tag{11}$$

Constraint C.4 (Table 2) is a positional constraint, therefore $k = 0$. When Eq. 5 is arranged to solve for bp_i the function coefficients and constant terms are given by Eq. 12 and Eq. 13 respectively.

$$a_{1,n} = [BP_{1,n} + BP_{2,n} \ldots + BP_{n-1,n}]C(\psi) \tag{12}$$

$$b_{1,0} = \xi - A_0 BP_{0,n} C(\psi) - A_n BP_{n,n} C(\psi) - \psi \Delta\xi_{te} \tag{13}$$

As the gradient is the first derivative of the $k = 1$ for constraint C.5 (Table 2). When Eq. 5 is solved for bp_i the function coefficients and constant terms are given by Eq. 14 and Eq. 15 respectively.

$$a_{2,n} = [BP_{1,n} + BP_{2,n} \ldots + BP_{n-1,n}]' C(\psi) + [BP_{1,n} + BP_{2,n} \ldots + BP_{n-1,n}] C'(\psi) \tag{14}$$

$$b_{2,0} = \xi'(\psi) - \Delta\xi_{te} - A_0 BP_{0,n} C'(\psi) - A_n BP_{n,n} C'\psi - A_0 BP'_{0,n} C_\psi - A_n BP'_{n,n} C_\psi \quad (15)$$

Similarly $k = 2$ for the second-derivative constraint C.6 (Table 2) and the the function coefficients and constant terms are given by Eq. 16 and Eq. 17 respectively.

$$a_{3,n} = [BP_{1,n} + BP_{2,n} \ldots + BP_{n-1,n}]'' C(\psi) + 2([BP_{1,n} + BP_{2,n} \ldots + BP_{n-1,n}]' C(\psi)') + [BP_{1,n} + BP_{2,n} \ldots + BP_{n-1,n}] C''(\psi) \quad (16)$$

$$b_{3,0} = \xi''(\psi) - A_0 BP_{0,n} C''(\psi) - A_n BP_{n,n} C''\psi - 2[A_0 BP'_{0,n} C'(\psi) + A_n BP'_{n,n} C'\psi] - A_0 BP''_{0,n} C_\psi - A_n BP''_{n,n} C_\psi \quad (17)$$

The Bernstein polynomial weighting coefficients are then given by Eq.18. All the Bernstein polynomial weighting coefficients have now been analytically calculated and the fan cowl profile fully defined (Figure 3). It can be seen that the fan cowl aero-line passes through the specified control points and fulfills the gradient and second-derivative constraints.

$$\mathbf{X} = \mathbf{A}^{-1} \cdot \mathbf{B} \quad (18)$$

Figure 4 shows a comparison of the original and the reconstructed fan cowl parametric geometry. The use of just the six main dimensions of the nacelle profile results in a shape that closely resembles the original. The largest difference between the shapes is 0.011 m on the rear part of the fan cowl, about 0.6% of local radius. This means that the parametric approach is able to provide a representative geometry which provides a good, slightly conservative estimate of the space available in the original design.

An intake was designed for the CRM aircraft cruise point, M=0.85 at an altitude of approximately 11,023m based on a wing chord Reynolds number of 40×10^6. The intake was sized for a mass-flow capture ratio of 0.75. A fan hub to tip of 0.3 [11] was assumed. These values in conjunction with a fan face Mach number of 0.6 [11] gave a fan diameter of 3.248m. The 1-dimensional average throat Mach number should be less than 0.75 [12]. A value of 0.72 was used to size the throat. The intake length was set by an L_{intake}/D_{fan} of 0.5. The intake aero-line was then created in a similar fashion to the fan cowl CST aero-line construction. Constraints for the intake include the position and the gradient and second derivative at the throat. The gradient and second derivative were also specified at the juncture with the nominal fan face (Figure 3). The maximum diffuser angle should not exceed 7^o to avoid diffusion driven separation within the intake [13]. The resultant design had an intake contraction ratio (CR) and lip aspect ratio (AR) of 1.26 and 2.65 respectively.

CFD methodology

The suitability of the proposed curve-fitting method for modeling nacelle geometries was tested by generating nacelle geometries, consisting of fan cowl and intake lines created from parametric CST curves using intuitive constraints. The aerodynamic performance of intakes and fan cowls was then assessed using two separate CFD approaches. Fan cowl performance was tested at a range of MFCRs and Mach numbers. To reduce the computational complexity for this initial evaluation of the approach, a 2D axisymmetric approach was adopted. Since intake performance is primarily assessed at off-design conditions, the high incidence aerodynamic performance of the intake has been tested using a 3D CFD approach, covering a range of incidence angles. Both the 2D and 3D CFD approaches are discussed in the following sections, together with the common CFD solver algorithm and model implemented.

CFD Solver

ANSYS Fluent v15 [14] was used as the CFD solver. Computations were carried out using the Reynolds-Averaged Navier-Stokes, implicit, density-based approach coupled with the SST $k-\omega$ turbulence model. Air was modeled as an ideal compressible gas according to kinetic theory. Variable viscosity was calculated using Sutherlands law. The solution method was a cell-centered implicit time-stepping scheme using the Roe-FDS scheme for flux calculation, and Green-Gauss node-based gradient evaluation. Second order, upwind discretizations were utilized for the convection terms. Solutions were deemed to be converged when all scaled residuals reached a value below 1×10^{-5} and forces on all walls were iteration-independent.

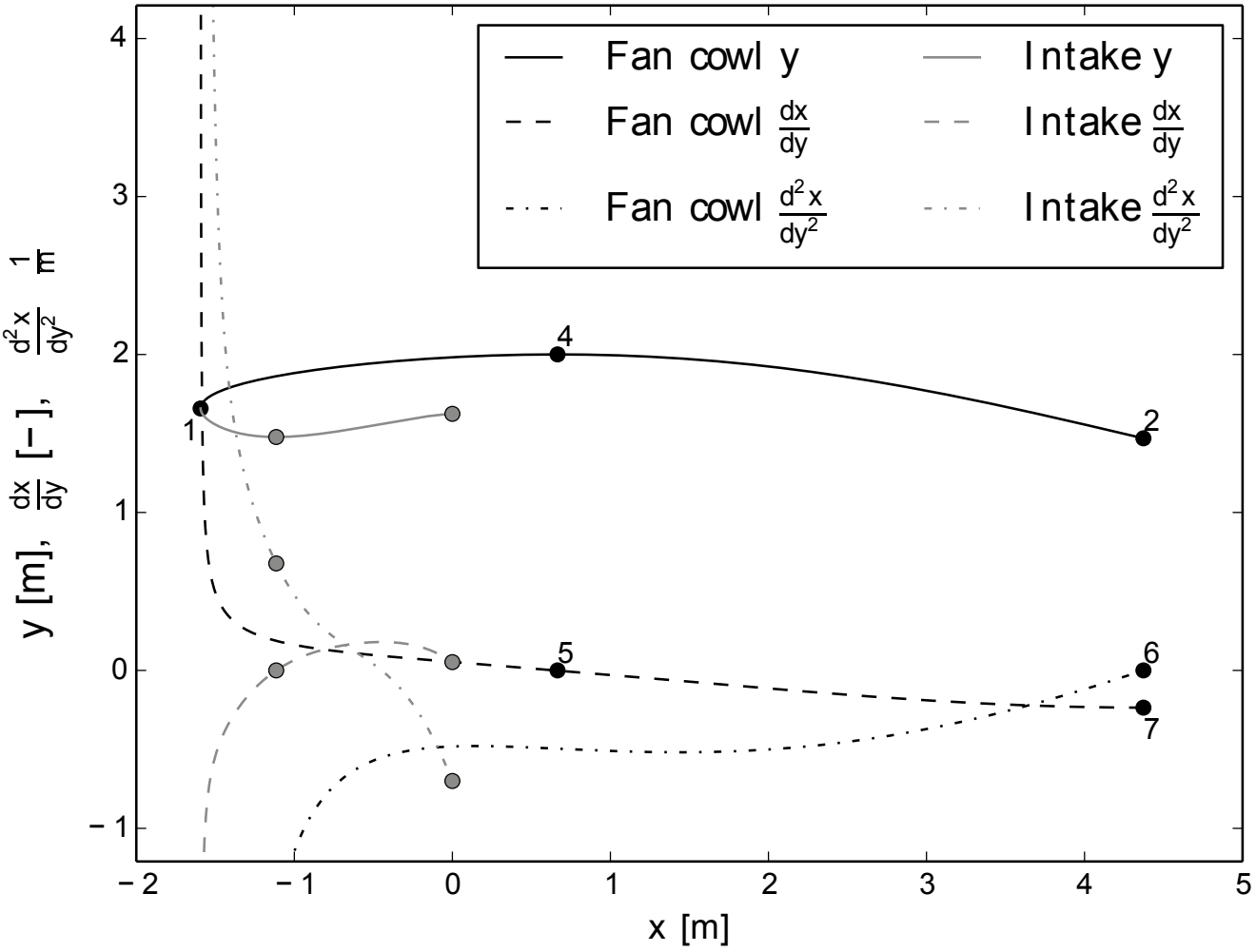

Fig. 3: Fan cowl and intake CST curves, their first and second derivatives and their constraints

2D axisymmetric CFD model

To represent an isolated axisymmetric nacelle in free-stream conditions, a 2D axisymmetric approach was used. The geometry incorporates both nacelle and intake aero-lines created using the parametric CST curves described in this paper, as well as a spinner. The use of a pressure-exit boundary condition at the position of the fan was found to cause convergence problems at incidence. For this reason and to limit the boundary condition influence on the fan face pressure profile, an aerodynamic interface plane (AIP) was defined in the fan location, and the domain extended by an annular duct. This duct ends 1.4 highlight radii downstream of the highlight in a pressure-exit boundary condition. Target mass-flow was specified at this station, causing the solver to iterate on the exit pressure to achieve predefined mass-flows. To achieve a neutral flow in the rear of the nacelle with minimal post-exit forces, a datum nozzle geometry was used, which consisted of a total-pressure inflow boundary condition and cylindrical, inviscid walls [15]. The total pressure specified was the same as on the far field, and thus the outflow velocity of the nozzle stream is equal to the ambient velocity [16]. The configuration is shown in Figure 5. A semi-circular far-field boundary was defined at 80 nacelle radii distance.

For meshing of 2D axisymmetric cases, ANSYS ICEM CFD [17] was used to create fully structured meshes for nacelle geometries. The boundary layer blocks normal to the fan cowl and intake use 50 cells. The first cell height was set to result in a $y_1^+ \approx 1$, with a stretching ratio of 1.2. To capture and resolve compressible shocks on the fan cowl, the maximum element size on the surface was limited to 1/110th of the nacelle length, resulting in 190 cells along the outside of a nacelle. The intake duct was resolved with 112 cells in radial direction. Figure 5 shows one of the 2D meshes used in this study, which has 46500 cells.

For each configuration, a range of Mach numbers and MFCRs was simulated, at constant Reynolds number $\approx 30 \times 10^6$ based on nacelle length. This corresponds to the CRM aircraft's cruise condition.

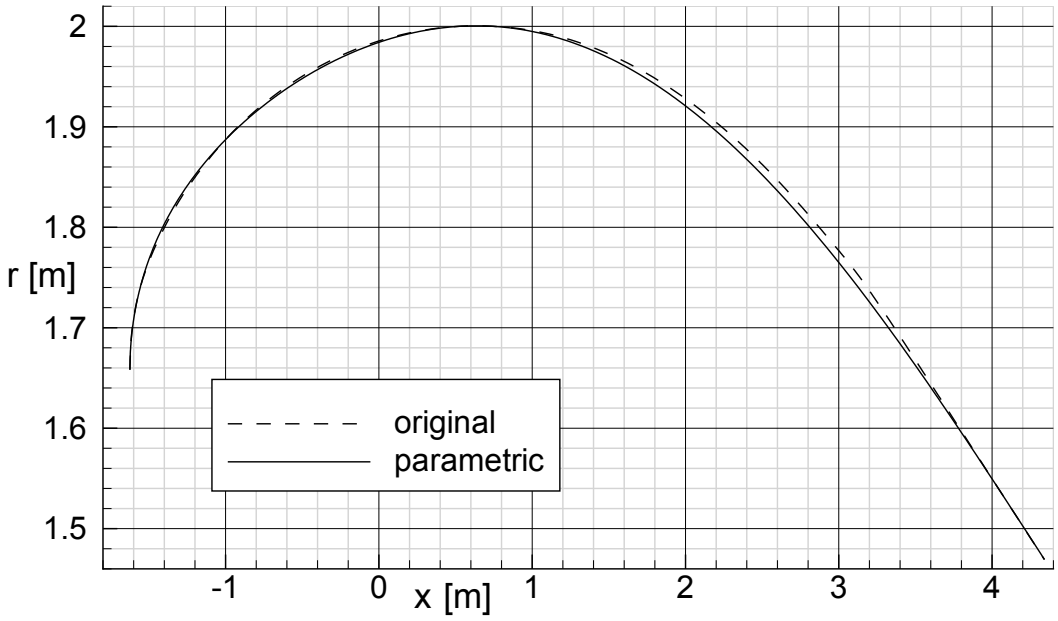

Fig. 4: Comparison of the original geometry of the CRM through-flow nacelle and the fan cowl line constructed using the parametric geometry.

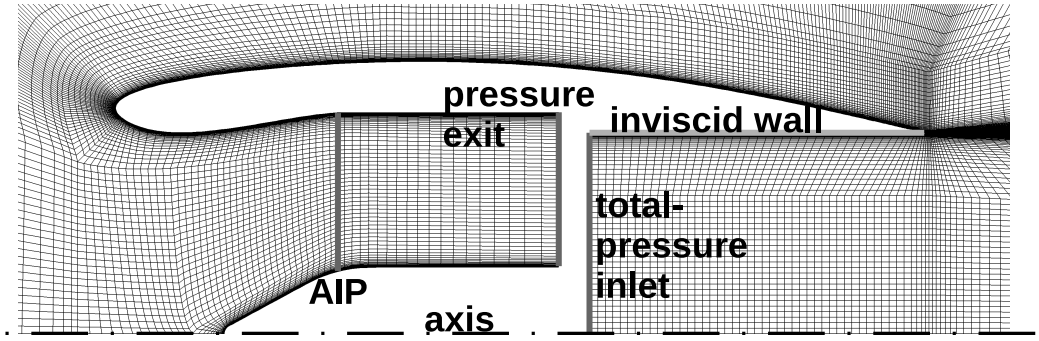

Fig. 5: View of one of the two-dimensional axisymmetric meshes used in this study, representing fan cowl and intake, including spinner

2D Domain and Mesh Convergence

Domain size and mesh density were based on the results of a domain sensitivity and mesh convergence studies for the very similar CFD model described in [10]. This resulted in a radius of the semicircular domain of 80 times the maximum nacelle radius. The Grid Convergence Index (GCI [18]) shows an upper bound of the discretization error on nacelle drag of less than 1%.

3D CFD model

A 3D CFD approach was implemented for the intake high-incidence performance calculations. 3D meshes were created with ANSYS ICEM CFD [17] using a fully-structured, multi-block approach (Figure 6). A boundary layer block was created at all solid boundaries across which there were 50 cells. The first cell height was set such that y^+ was approximately equal to 1. Minimum values of $2 \times 2 \times 2$ determinants and equi-angle skewness of 0.45 and 0.3 respectively were maintained. Boundary conditions were the same as those imposed in the 2D axisymmetric approach (Figure 7). The pressure outlet boundary was moved further downstream from the fan to limit its influence on the nominal fan face plane and to aid convergence.

3D Mesh Independence study

The datum 3D structured mesh was produced in ICEM v15.0 and consisted of 4.8 million cells. A mesh independence study was carried out using the recommended approach by Roache [18]; the GCI was calculated for three meshes with 2.4, 4.8 and 9.6 million elements. The GCI for nacelle drag for the coarsest and finest meshes were 0.73% and 0.05%,

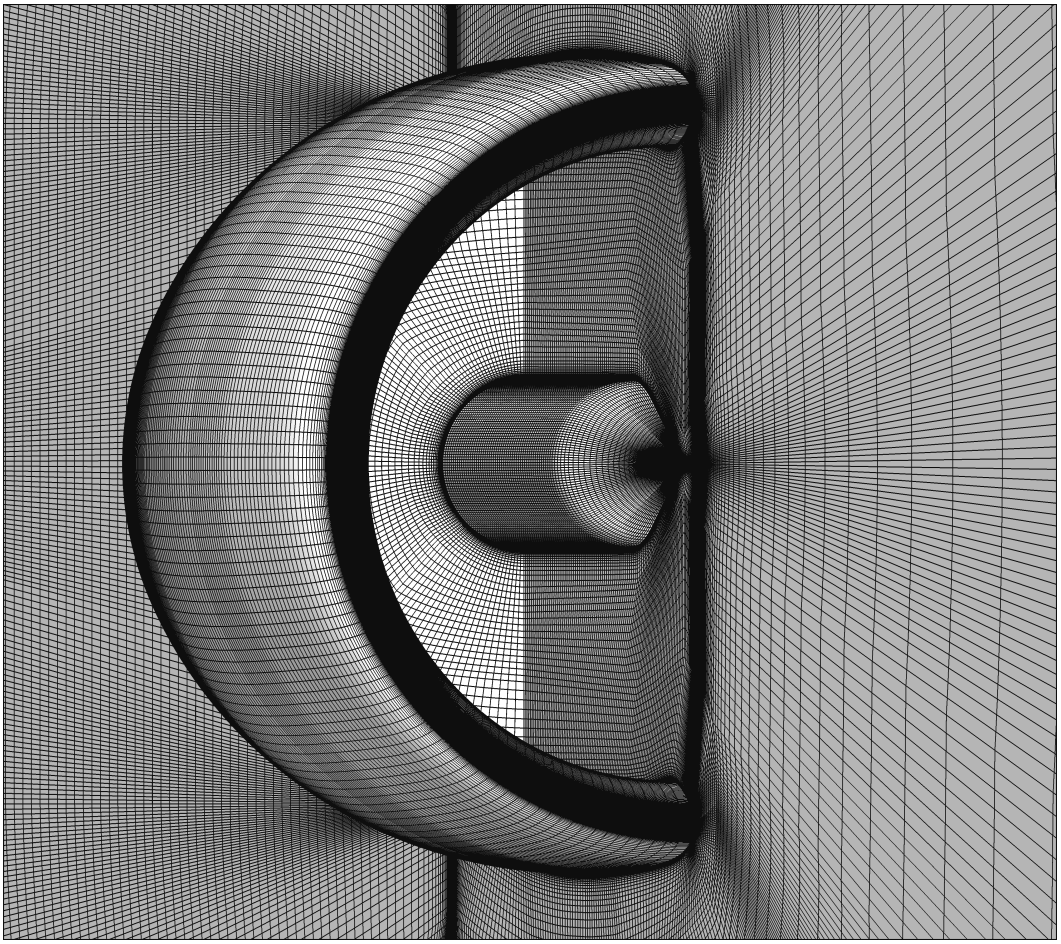

Fig. 6: 3D mesh

respectively. This meant that the medium grid was within a band of error, with regards to nacelle drag, greater than 0.05% and below 0.73% and resulted in a mesh size of 4.8 million elements.

Fan cowl performance assessment methodology

To assess fan cowl drag, the method shown by Christie [15] was used, which extracts the modified standard nacelle drag [16]. It uses surface integrals, velocity and pressure distribution on the AIP and the far-field state to compute the sum of the forces on the pre-entry streamtube and the fan cowl, ignoring forces on the post-exit streamtube. Nacelle drag figures in this paper are given as drag coefficients relative to the nacelle highlight area, using far-field dynamic pressure.

It was tested how closely the aerodynamic performance of a simple parametric fan cowl can approximate that of an existing design of equal proportions. This comparison regards modified standard nacelle drag at the main operating conditions for which fan cowls are designed. The criteria used are drag at mid-cruise, drag increase between mid-cruise and end-of-cruise condition and the drag rise Mach number. The mid-cruise condition was taken to be M=0.85 with a MFCR=0.75, consistent with the design condition of the CRM and the mass-flow through the TFN at design condition. The end-of-cruise operating condition is at equal Mach number but lower MFCR than mid-cruise, but is not exactly known for the CRM. While it was estimated that MFCR=0.70 would be realistic, a series of different MFCR was regarded which allows more general assessment of spillage behavior at cruise Mach number. The drag rise Mach number limits the Mach number range at which a nacelle can be economically operated and is defined as the point at which drag gradient over Mach number reaches a certain gradient. This paper uses $\frac{dc_D}{dM} = 0.05$. This was investigated by regarding drag as function of Mach number at cruise MFCR of 0.75.

The CFD data on which the analysis is based was generated by simulating the flow over an array of 224 different combinations of Mach number and MFCR spanning Mach numbers between 0.2 and 0.95, and MFCR between 0.3 and 95% of the choking intake mass-flow, at a constant Reynolds number of about $30 \cdot 10^6$. The results interpolating between them to cover the entire space of operating conditions. The drag curves shown in this report are slices of this interpolated data.

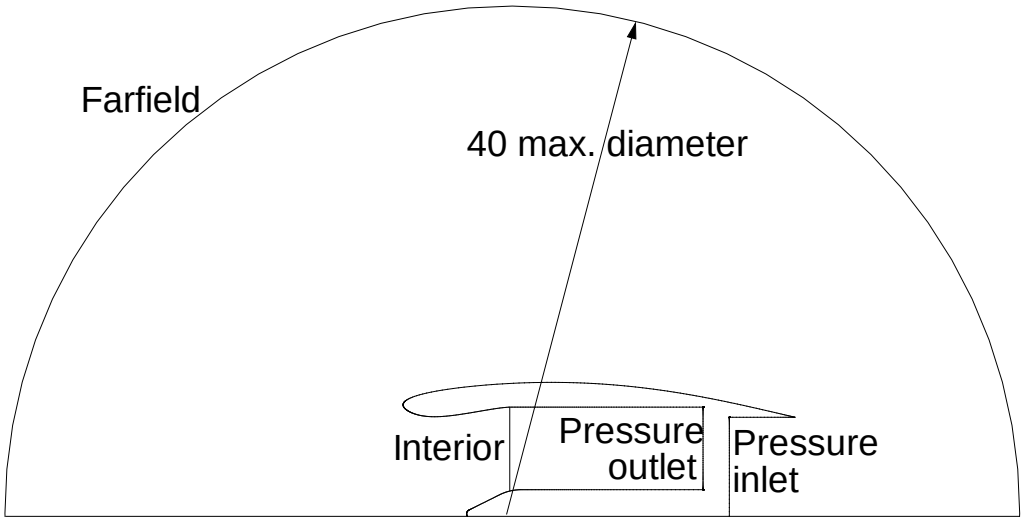

Fig. 7: 3D domain

Intake performance assessment methodology

A 3D intake was developed to demonstrate the potential usefulness of the CST parameterisation method. Four metrics have been used to judge the aerodynamic performance of aero-engine intakes. Intake Pressure Recovery (Eq. 19) is a measure of the total pressure losses in the intake due to viscous effects and shock losses.

$$IPR = \frac{\overline{P}_{0,fan\,face}}{P_0} \tag{19}$$

where:

$\overline{P}_{0,fan\,face}$ is the mean total pressure on the fan face
P_0 is the freestream total pressure

Area-weighted averaging is commonly used to calculate IPR [19]. Total pressure distortion is quantified using the DC_{60} correlation parameter (Eq. 20).

$$DC_{60} = \frac{P_{60} - \overline{P}_{0,fan\,face}}{q} \tag{20}$$

where:

P_{60} is the mean total pressure in the 60^o sector with the lowest mean total pressure
q is the dynamic pressure

To put calculated values of DC_{60} in context, a typical upper limit on DC_{60} is -0.2 for a civil subsonic transport aircraft. [20] An ideal intake design would exhibit no flow separation throughout its operating envelope. For all intake designs studied in this work, the presence and extents of flow separations have been assessed. Finally the maximum isentropic Mach number is used as a measure of flow acceleration around the intake lip. As incidence is increased flow accelerates around the intake lip followed by a rapid local diffusion often associated with the formation of a shockwave. This can cause a separation of the boundary layer and a degradation of intake aerodynamic performance.

RESULTS

The results section comprises three parts. Firstly, the aerodynamic performance of the fan cowl is assessed at zero incidence. Secondly, an assessment is made of the aerodynamic performance of the intake operating at high incidence with a axisymmetric geometry and 3D CFD. Finally, a brief description of a more detailed application of the parametric method to short intakes is provided.

Nacelle drag characteristics

The drag characteristics of the reconstructed parametric fan cowl were compared to that of the original CRM nacelle sidelines. Being a low-order approximation of the original design and aimed at preliminary design scenarios, it is expected that the parametric shape will have slightly reduced performance. In order to be well-suited to its purpose, however, the offset needs to be consistently small.

Figure 8 shows the drag rise curves at MFCR=0.75. It can be seen that the parametric geometry provides both a slightly increased drag rise Mach number, by about 0.002, and a small reduction of drag at all Mach numbers at MFCR=0.75, by about 1.5%.

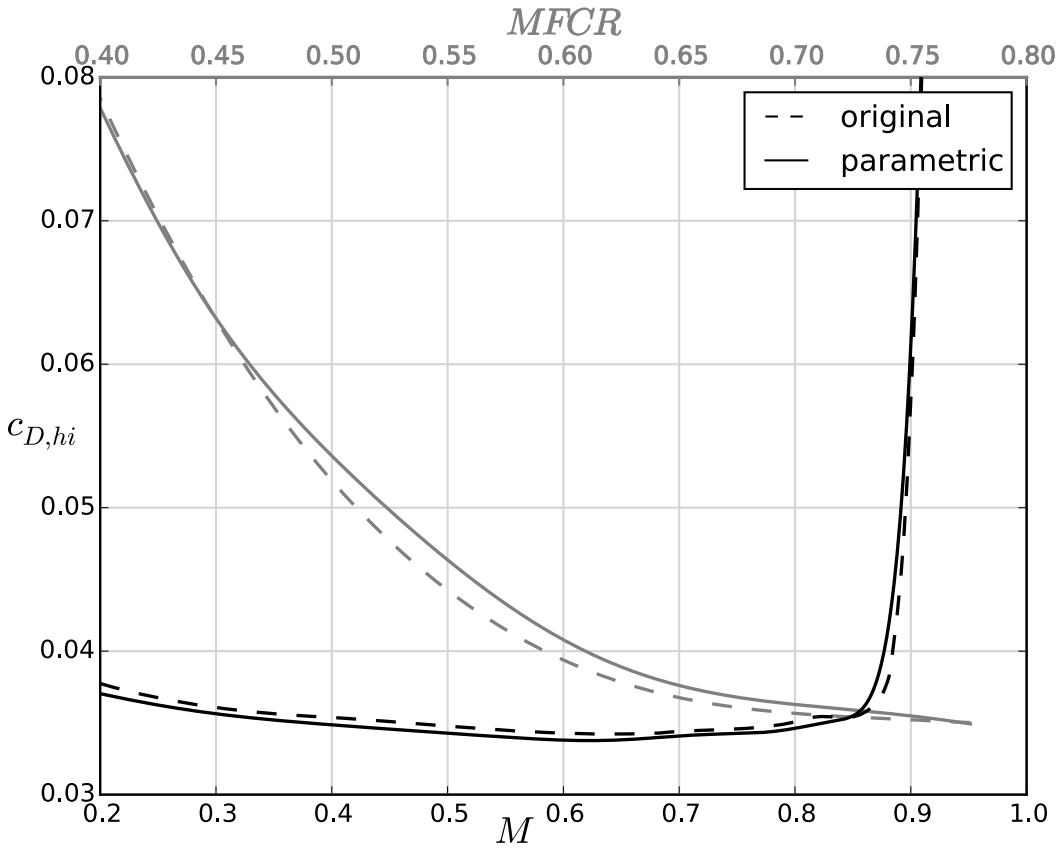

Fig. 8: Comparison of drag rise curves for the original and the reconstructed parametric shape, at mid-cruise mass-flow capture ratio of 0.75, and spillage curve at cruise Mach number (0.85).

Figure 8 also shows a variation of MFCR at a constant Mach number of $M = 0.85$. This curve shows that the parametric fan cowl has worse spillage behavior than the original geometry, with about 7% increase in drag for mass-flow capture ratios around 0.5.

This is a fairly close approximation of the original drag characteristics, and it is plausible to assume that there are small design changes, e.g. to the initial forebody radius, which could sacrifice some baseline drag or reduce drag rise Mach number to achieve better spillage behavior, bringing the performance even more in line. Overall it can be seen that despite the limited inputs and no design iterations, the aerodynamic performance of the parametric fan cowl is close to that of an existing design. This demonstrates both the ability of CST curves to produce aerodynamically favorable shapes and the usefulness of the chosen approach in the creation of parametric geometries. The method presented in this paper is thus shown to be a very efficient way of creating shapes which are useful in preliminary design environments, either to represent shapes for which no detailed design is available, or as a starting point for a more in-depth design process.

Intake high incidence performance

Besides the assessment of the nacelle drag characteristics with 2D CFD, the high incidence performance of the intake was assessed with 3D CFD. This was carried out to test the aerodynamic performance capability of the parametrically defined

intake at high incidence. A 3D axisymmetric geometry was constructed from the parametrically defined intake and fan cowl aero-lines (Figure 3).

The off-design wing C_{Lmax} condition features the largest angle of attack which the engine can be subjected to in flight [21]. This operating condition is not encountered in a typical flight, but it is important to demonstrate high incidence intake performance capability at this operating point as part of the certification process. The high incidence capability of the intake is typically tested at a Mach number of 0.25 [21]. All intake simulations in this paper have been carried out at conditions equivalent to an altitude of 16,600ft. The performance of the parametrically defined intake has been assessed with the previously discussed performance metrics; DC_{60}, IPR and M_{isen}. An assessment of the sensitivity to engine angle of attack was performed for a range of engine angle of attack from 22^o to 29^o. At 29^o a substantial intake separation arose. At 22^o engine angle of attack no flow separations were present in the intake. Intake pressure recovery and maximum isentropic Mach number were calculated to be 0.999 and 0.99 respectively (Figure 9). The DC60 correlation parameter, which gives a measure of total pressure distortion at the fan face was calculated to be -0.02.

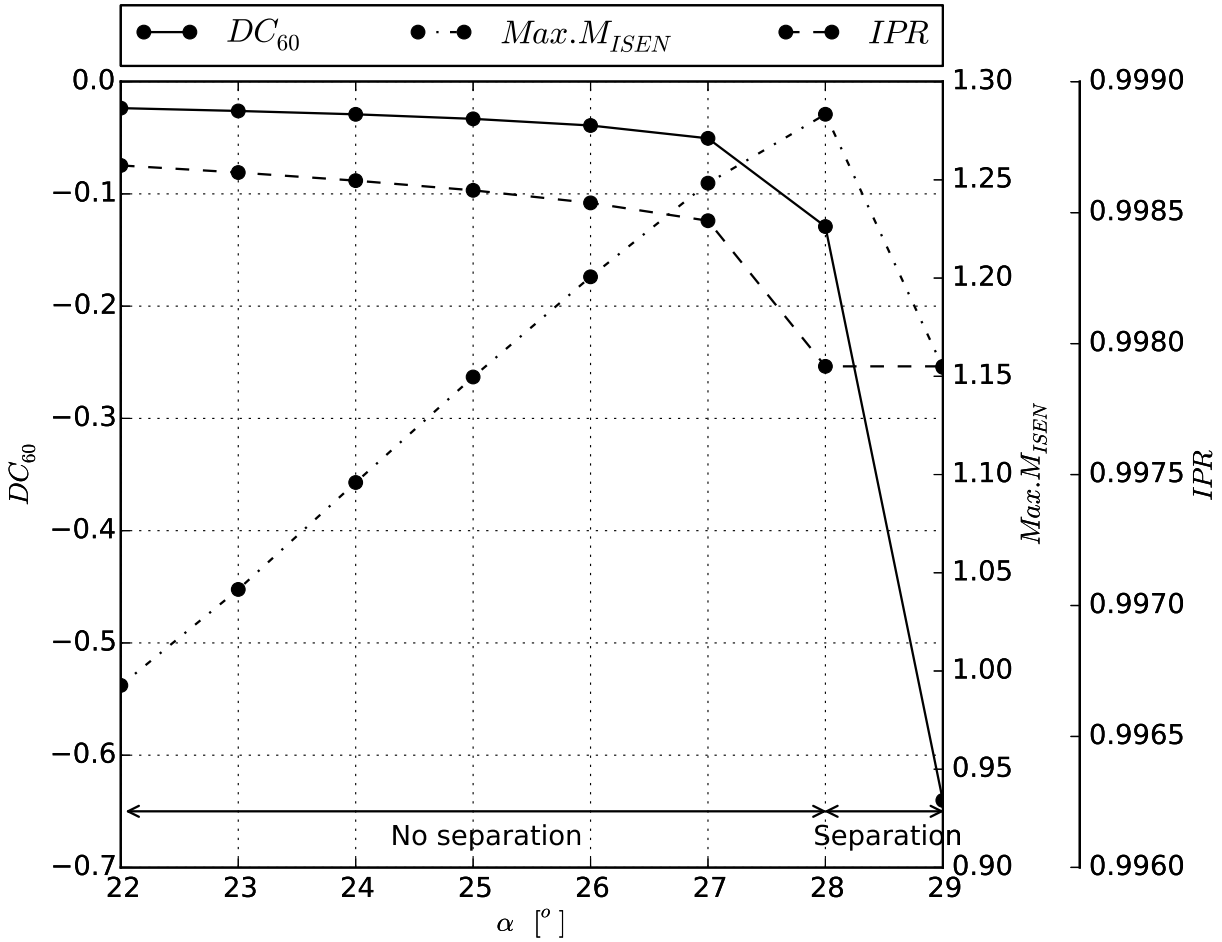

Fig. 9: Variation of DC_{60}, maximum M_{ISEN} and IPR with changes in α, M=0.25, Alt.=16,600ft, MFCR=1.4.

As the engine angle of attack is increased from 22^o to 27^o, DC_{60} and maximum isentropic Mach number increase while IPR decreases. At $\alpha = 22^o$ there is no lip shock (Figure 10a) but as α is increased the maximum isentropic Mach number around the lip increases (Figure 11) with a peak at $\alpha = 28^o$ where there is a clear single shock (Figure 10b). No separation of the intake flow occurs until an angle of attack of 28^o (Figure 12). At this angle of attack, a small shock induced separation arises although it quickly reattaches with a separation length on the order of $3 \times 10^{-3} L_{intake}$. A second region of reverse flow due to a diffusion induced separation extends through the fan face. The effect of this reverse flow can be seen in the distributions of total pressure on the fan face (Figure 12) and the increase in DC_{60} magnitude (Figure 9). At an angle of attack of 29^o the diffusion driven separation has increased substantially in size and augmented total pressure losses over much of the nominal fan face. There is an order of magnitude increase in DC_{60} between an angle of attack of 28^o and 29^o from -0.13

to -0.64. This is outside the acceptable range of fan face distortion and may be large enough to trigger surge [22].

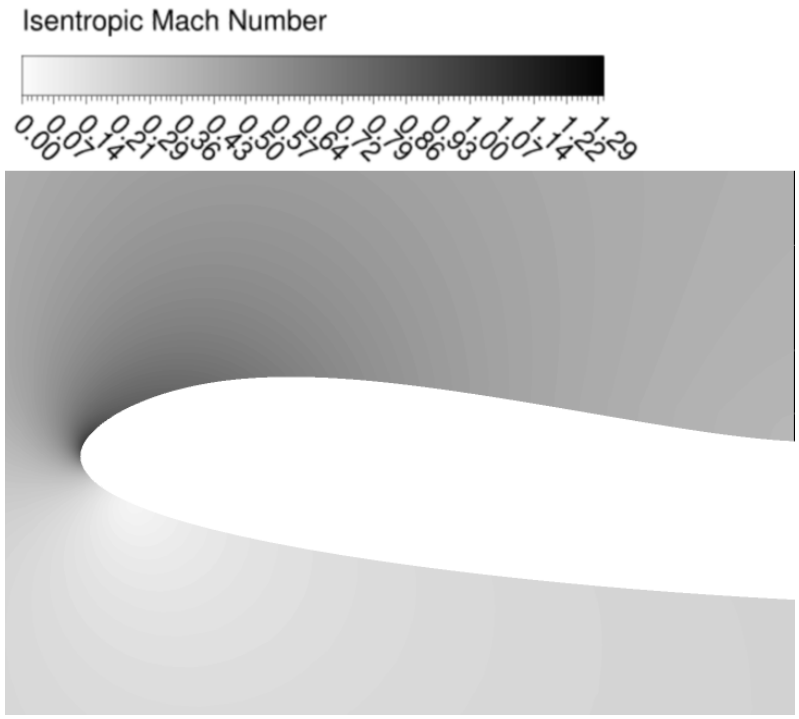

(a) $\alpha = 22^o$

(b) $\alpha = 28^o$

Fig. 10: Mach number distributions around the lower lip (180^o from TDC) of the parametrically defined intake at different angle of attack, M=0.25, Alt.=16,600ft, MFCR=1.4.

The reasonable aerodynamic performance of the bottom aero-line of the parametrically defined intake demonstrates the capability of the intake parameterisation method. No design iterations have been carried out. With further design iterations and modifications to the intake parameterisation method to increase intake lip curvature control it is possible improve the intake aerodynamic performance. A smooth monotonic change in curvature can be achieved from the highlight point to the throat and this can eliminate the double shock flow topology seen at lower angle of attack for the parameterized intake ($22^o \leq \alpha \leq 24^0$). When this is achieved the flow remains attached for longer around the lip and the maximum isentropic Mach number is reduced. To further illustrate the utility of the intake parameterisation method the following section briefly discusses the design development of a short intake based on the iCST methodology.. This demonstrates the effects of several

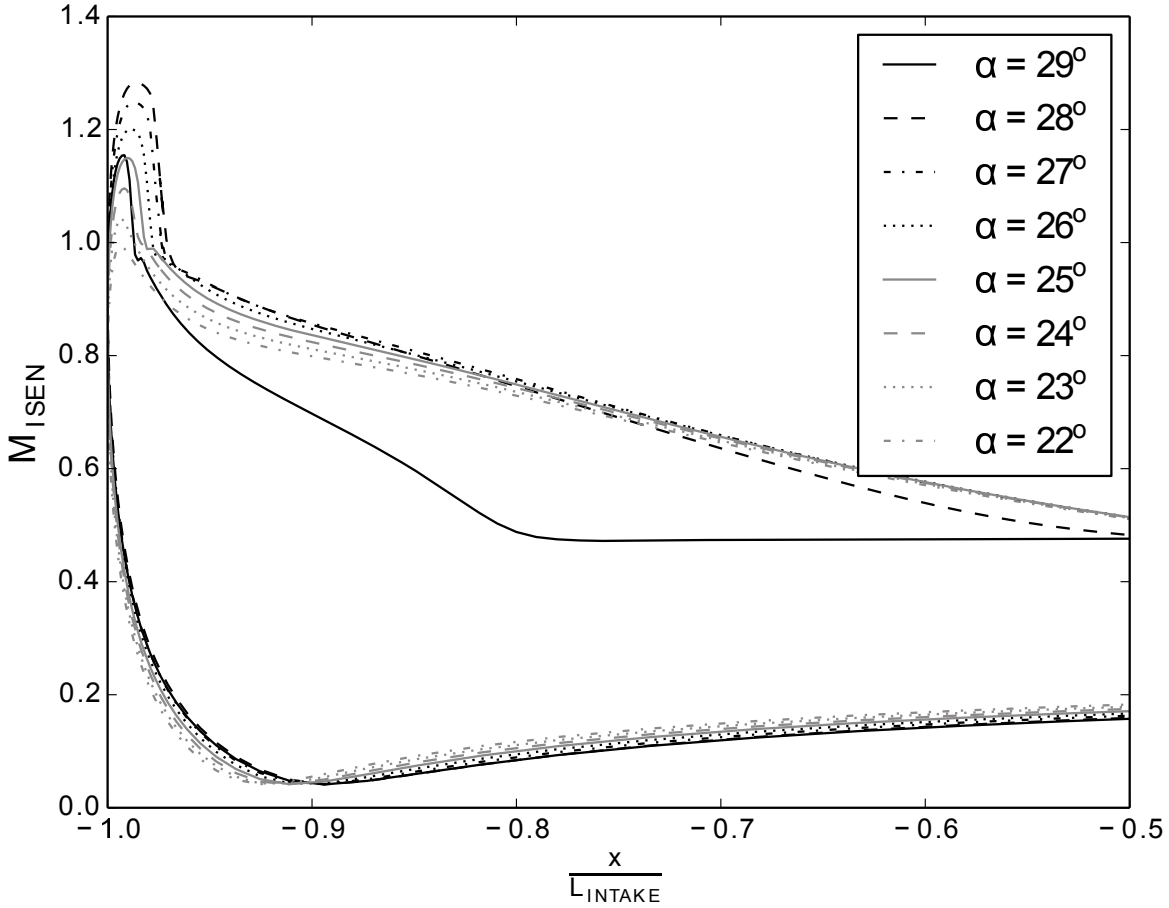

Fig. 11: Variation of isentropic Mach number around the bottom lip with changes in α, M=0.25, Alt.=14,000ft, MFCR=1.62.

design iterations and the effect of increased lip curvature control on intake performance for a challenging design.

Short intake high incidence performance

As fan pressure ratio (FPR) is decreased to improve fuel burn, reduce emissions and noise, the fan diameter grows and innovative nacelle concepts including short inlets are required to reduce weight and drag. However decreased inlet length can potentially result in reduced diffusion capability and increased flow non-uniformity at the fan face which impacts upon fan performance. The challenge is then to design shorter intakes without compromising intake and fan performance.

The intake design approach outlined in "Example test case" was used as a starting point in the design of a baseline short intake, (Intake A), with an intake length over fan diameter (L_{intake}/D_{fan}) of 0.35. This is relative to a conventional intake with an L_{intake}/D_{fan} of 0.5. However in order to reduce the maximum diffuser angle below 7^o the CR was reduced to 1.15. Despite an acceptably low maximum isentropic Mach number over the lip ($M = 1.35$), a large shock induced separation was seen (Figure 13 and 14). This shock induced separation did not reattach before the diffuser and extended through the fan face. The incurred losses resulted in a low intake pressure recovery of 0.970 and a high DC_{60} of -0.56 (Table 3). This inadequate intake performance highlighted the need to move away from standard intake design guidelines for M_{TH}, CR and AR. It also showed that care needed to be taken in controlling the flow acceleration around the lip to minimize or remove shock induced separation.

Intake B was designed with the same intake parameterisation as Intake A, but with some iteration on the intake parameters to improve aerodynamic performance. For this intake the *IPR* and maximum M_{isen} were calculated to be 0.996 and 1.37 respectively (Table 3). The DC_{60} parameter was calculated to be -0.05. Two small regions of reverse flow were present in the intake. There was an initial small region of reverse flow in the shock induced separation (Figure 13 and 14). The second region of reverse flow due to a diffusion induced separation extended through to the fan face. The effect of this reverse flow can clearly be seen in the distributions of total pressure on the fan face (Figure 13 and 14).

A need to improve curvature control around the intake lip was identified. Intake C was designed to have a monotonic change in curvature from the highlight to the throat. This was achieved through the use of a "hybrid-CST" intake. It is

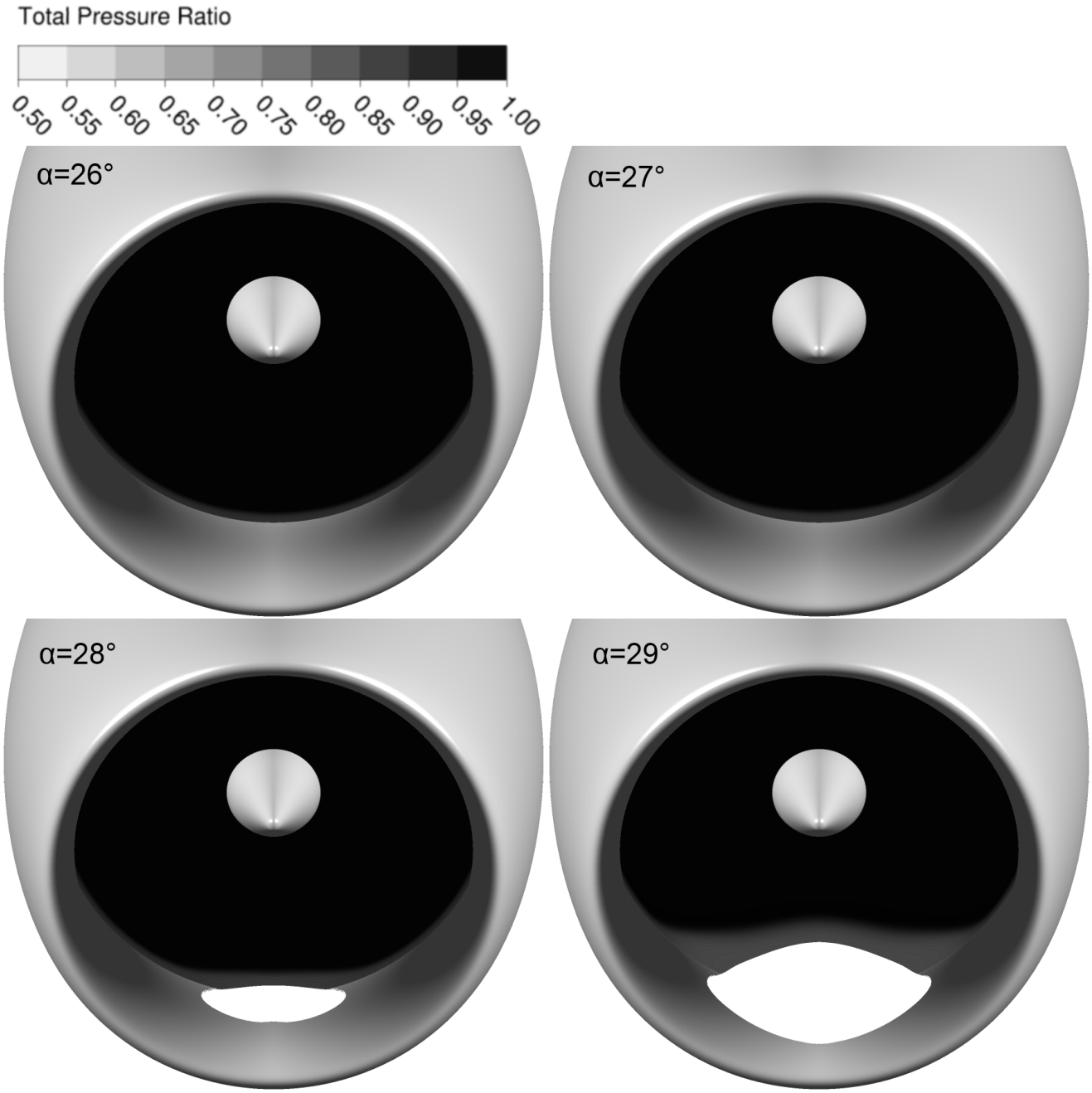

Fig. 12: Variation of total pressure ratio on the nominal fan face with changes in α, M=0.25, Alt.=16,600ft, MFCR=1.4. Iso-surfaces of zero axial velocity are shown in white to illustrate areas of separation.

an inherent property of CST curves that their infinite derivatives are continuous [3]. This means that even if the gradient and curvature are specified and fixed at the throat, changes to the diffuser shape will result in changes in the lip shape. To allow more control over the curvature distribution around the lip two CST curves are used to create the intake. Both go from the highlight to the fan face and have common constraints at the throat point where they intersect. This approach was employed to allow the diffuser design to be altered independently of the lip design and vice-versa. In this manner a smooth monotonic change in curvature can be achieved from the highlight point to the throat. As gradient and curvature are fixed at the throat point the intake has continuous curvature from the highlight to the fan face but is discontinuous in rate of change of curvature at the throat. Due to the improved lip design, where a smooth monotonic increase in lip curvature was specified, the maximum isentropic Mach number was reduced from 1.36 to 1.25 relative to Intake B at the same conditions (Table 3). This reduction in maximum isentropic Mach number over the lip removed the shock induced separation that was present for Intake B. The only separation present was a small diffusion induced separation which reattached before the fan face (Figure 13).

This design exercise assessed the capability of the intake parameterisation method at a realistic but challenging design point. The reasonable aerodynamic performance of this intake bottom aero-line demonstrates the capability of the intake parameterisation method.

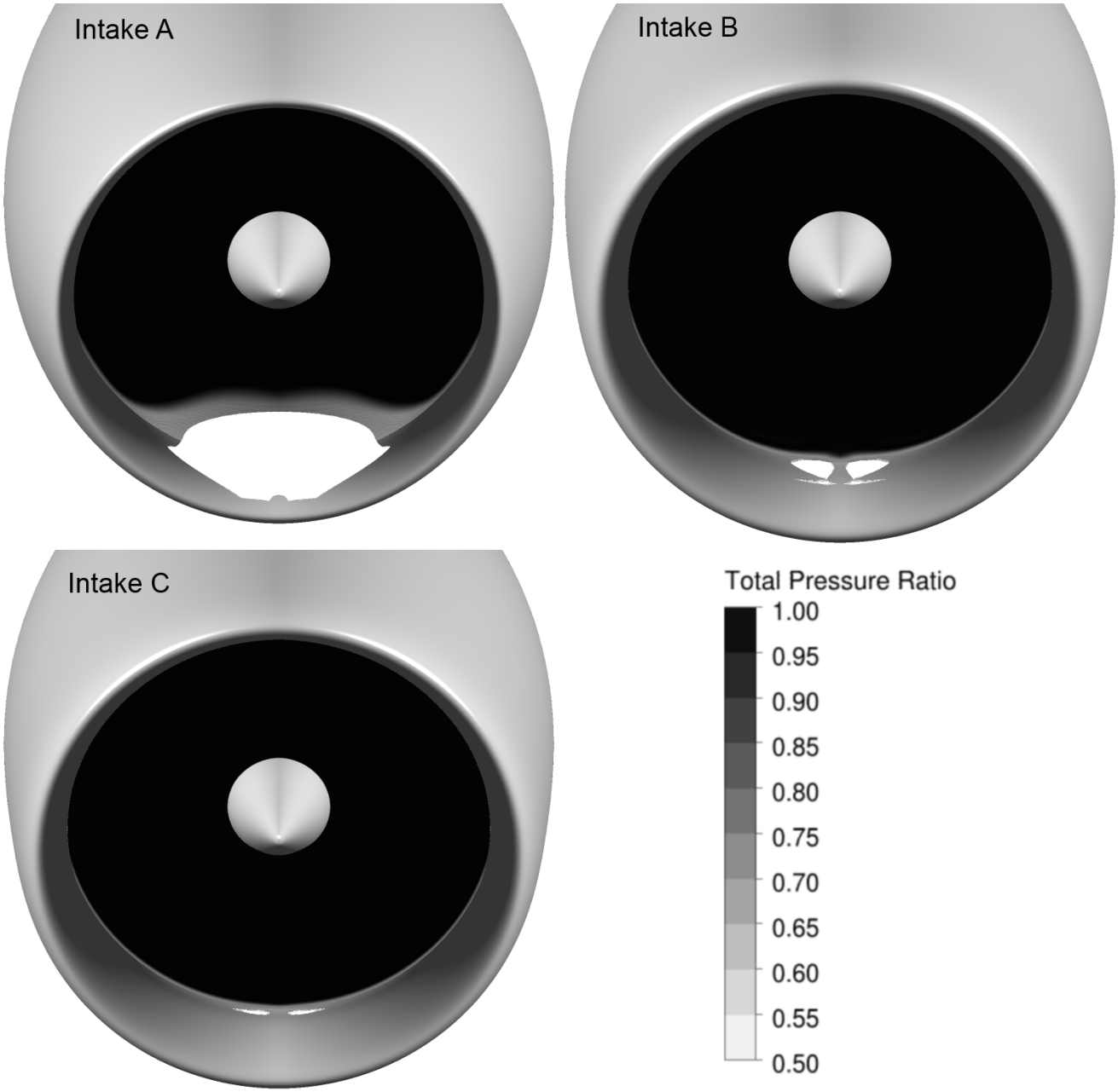

Fig. 13: Variation of total pressure ratio on the nominal fan face for short intakes A, B and C. M=0.25, alt.=16,600ft, $\alpha = 22^o$, Q_{fan} equal to that of the conventional length intake. Iso-surfaces of zero axial velocity are shown in white to illustrate areas of separation

CONCLUSIONS

The method presented in this paper allows the analytical calculation of a transformation matrix which allows a CST parameterized fan cowl and intake to be fully defined by aerodynamically intuitive design variables. It was also demonstrated that this approach can be used to quickly create fan cowl and intake geometries which have adequate aerodynamic performance with a limited set of intuitive design parameters. The approach allows different aero-line parameterisation schemes

Intake	A	B	C
DC_{60}:	-0.56	-0.05	-0.03
IPR:	0.970	0.996	0.996
Max. M_{ISEN}:	1.35	1.37	1.25

Table 3: Intake performance metrics for Intakes A, B and C

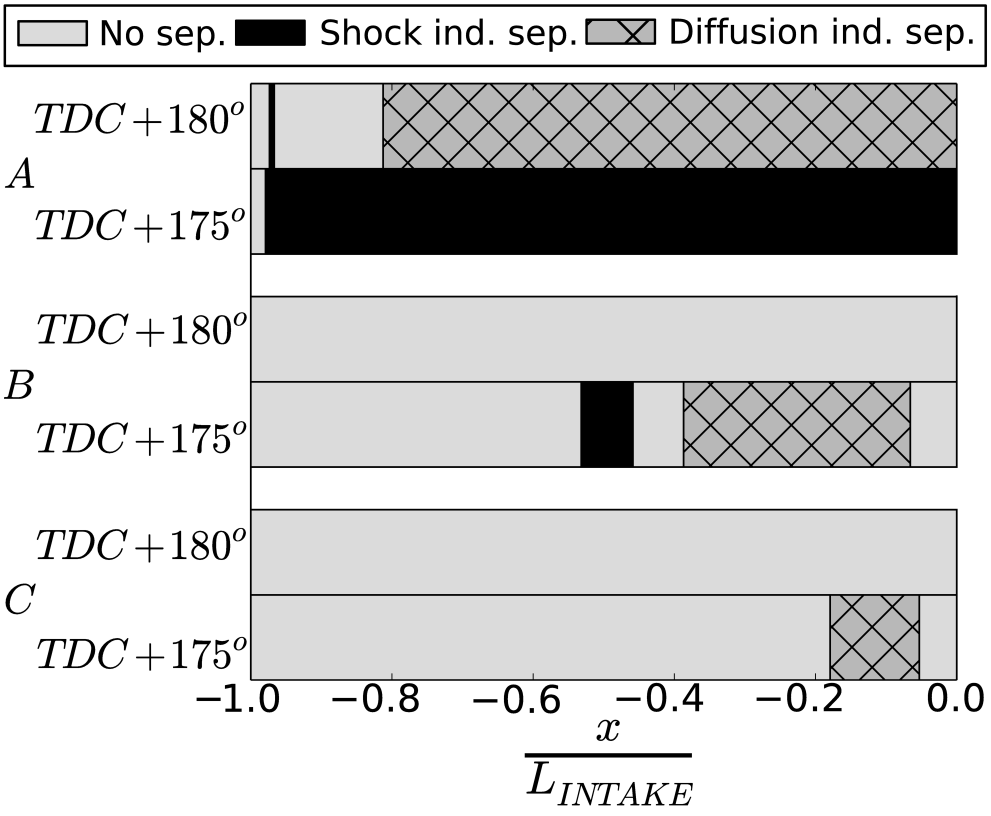

Fig. 14: The extent and initial cause of intake separations for short intakes A, B and C. M=0.25, alt.=16,600ft, $\alpha = 22^o$, Q_{fan} equal to that of the conventional length intake.

to be rapidly implemented and allows for very quick generation of geometries. A nacelle geometry with a conventional length intake (L_{intake}/D_{fan}=0.5) was generated based only on the main geometric dimensions of the CRM TFN. The high incidence intake performance capability of the 2D axisymmetric, parametrically defined geometry was assessed with 3D CFD. The reasonable aerodynamic performance of this parametrically defined intake bottom aero-line demonstrates the capability of the intake parameterisation method. Reasonable drag characteristics were demonstrated for this nacelle with 2D axisymmetric CFD. This shows that adequately performing fan cowl and intake aero-lines can be constructed with the CST parameterisation outlined in this work. A short intake (L_{intake}/D_{fan}=0.35) was designed using a larger number of intuitive design variables than for the conventional length intake, necessitated by the use of a "hybrid-CST" intake. This shows that the method can also be used in detailed design. Overall, this tool is suited for shape generation in preliminary and detailed design and optimization of geometry definitions for fan cowls and intakes.

Acknowledgements

This project was co-funded by Innovate UK.

References

[1] Straathof, M. H., Van Tooren, M. J., Voskuijl, M., and Koren, B., 2008. "Aerodynamic shape parameterisation and optimisation of novel configurations". In The Aerodynamics of Novel configurations: capabilities and future requirements. Proceedings of the 2008 Royal Aeronautical Society Annual Applied Aerodynamics Research Conference, London, 27-28 October,(2008), Royal Aeronautical Society.

[2] Anderson, G., Aftosmis, M., and Nemec, M., 2012. "Constraint-based shape parameterization for aerodynamic design". In 7th International Conference on Computational Fluid Dynamics, Big Island, Hawaii.

[3] Kulfan, B. M., and Bussoletti, J. E., 2006. "Fundamental parametric geometry representations for aircraft component shapes". In 11th AIAA/ISSMO multidisciplinary analysis and optimization, AIAA-2006-6948.

[4] Kulfan, B. M., 2008. "Universal parametric geometry representation method". *Journal of Aircraft,* **45**(1), pp. 142–158.

[5] Zhu, F., and Qin, N., 2013. "Intuitive class/shape function parameterization for airfoils". *AIAA Journal,* **52**(1), pp. 17–25.

[6] Sobieczky, H., 1999. "Parametric airfoils and wings". In *Recent Development of Aerodynamic Design Methodologies*. Springer, pp. 71–87.

[7] Vassberg, J. C., DeHaan, M. A., Rivers, S. M., and R. A. Wahls, R. A., 2008. "Development of a Common Research Model for Applied CFD Validation Studies". In 26th AIAA Applied Aerodynamics Conference, 2008-6919, American Institute of Aeronautics and Astronautics, AIAA.

[8] Certik, O., et al., 2008. Sympy python library for symbolic mathematics. Tech. rep., Technical report (since 2006), http://code. google. com/p/sympy/(accessed November 2009).

[9] Newville, M., Stensitzki, T., Allen, D., and Ingargiola, A., 2014. Lmfit: Non-linear least-square minimization and curve-fitting for python. zenodo.

[10] Heidebrecht, A., Stańkowski, T., and MacManus, D., 2016. "Parametric geometry and computational process for turbofan nacelles". In ASME Turbo Expo, ASME. GT2016-57784.

[11] Walsh, P. P., and Fletcher, P., 2004. *Gas turbine performance*. Blackwell Scientific Publications, Oxford.

[12] Farokhi, S., 2014. *Aircraft propulsion*. Wiley, New York.

[13] Chandavari, V., and Palekar, M. S., 2014. "Diffuser angle control to avoid flow separation". *International Journal of Technical Research and Applications,* **2**, pp. 16–21.

[14] ANSYS, 2014. "Fluent users guide".

[15] Christie, R., Ramirez, S., and MacManus, D. G., 2014. "Aero-engine installation modelling and the impact on overall flight performance". In Advanced Aero Concepts, Design and Operations, Royal Aeronautical Society.

[16] MIDAP Study Group, 1979. Agardograph no. 237 guide to in-flight thrust measurement of turbojets and fan engines. Tech. Rep. AG-237, AGARD.

[17] ANSYS, 2014. "ICEM CFD 15.0 Users Manual".

[18] Roache, P., 1998. *Verification and validation in computational science and engineering*. Hermosa publishers.

[19] Goldsmith, E. L., and Seddon, J., 1993. *Practical intake aerodynamic design*. AIAA Education Series.

[20] Lee, K., Lee, B., Kang, S., Yang, S., and Lee, D., 2010. "Inlet distortion test with gas turbine engine in the altitude engine test facility". *AIAA Paper,* **4337**, p. 2010.

[21] Peters, A., Spakovszky, Z. S., Lord, W. K., and Rose, B., 2015. "Ultrashort nacelles for low fan pressure ratio propulsors". *Journal of Turbomachinery,* **137**(2), p. 021001.

[22] Rademakers, R. P., Bindl, S., and Niehuis, R., 2016. "Effects of flow distortions as they occur in s-duct inlets on the performance and stability of a jet engine". *Journal of Engineering for Gas Turbines and Power,* **138**(2), p. 022605.